Ultrafast Wiggling and Jiggling: Ir_2(1,8-diisocyanomenthane)$_4^{2+}$

Martin Pižl,[a,b] Bryan M. Hunter,[c] Gregory M. Greetham,[d] Michael Towrie,[d] Stanislav Záliš,[a,*] Harry B. Gray,[c,*] Antonín Vlček[a,e,*]

[a] J. Heyrovský Institute of Physical Chemistry, Academy of Sciences of the Czech Republic, Dolejškova 3, CZ-182 23 Prague, Czech Republic
[b] Department of Inorganic Chemistry, University of Chemistry and Technology, Prague, Technická 5, CZ-166 28 Prague, Czech Republic
[c] Beckman Institute, California Institute of Technology, Pasadena, CA 91125, USA
[d] Central Laser Facility, Research Complex at Harwell, STFC, Rutherford Appleton Laboratory, Harwell Oxford, Didcot, Oxfordshire OX11 0QX, United Kingdom,
[e] Queen Mary University of London, School of Biological and Chemical Sciences, Mile End Road, London E1 4NS, United Kingdom
e-mail: zalis@jh-inst.cas.cz, hbgray@caltech.edu, a.vlcek@qmul.ac.uk

SUPPLEMENTARY INFORMATION

Contents

FIGURES

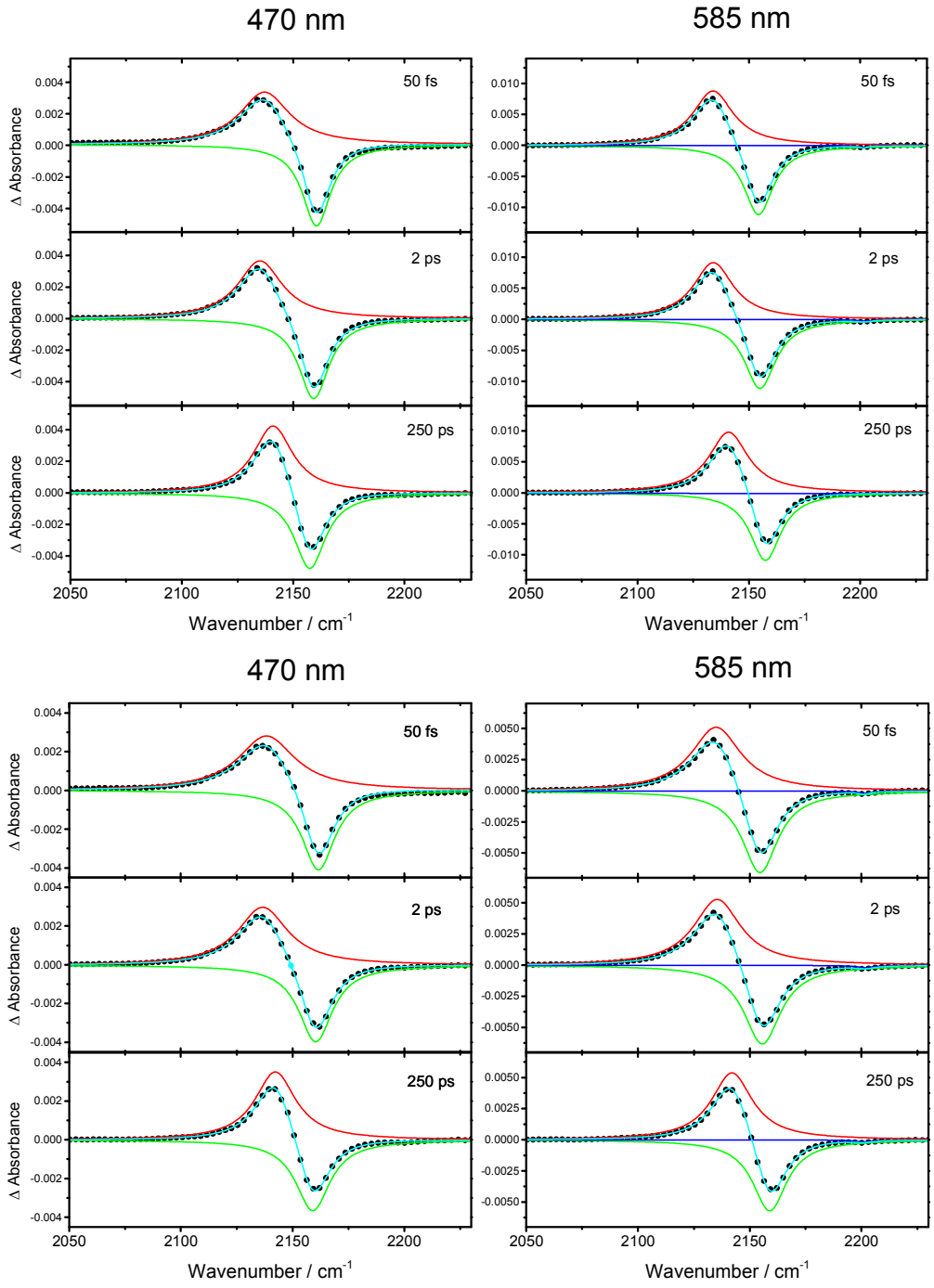

Figure S1. Representative Lorentzian fits of Ir(dimen) TRIR spectra in DCM (top) and MeCN (bottom). 470 nm – excited spectra (left) fitted with two Lorentzians, 585 nm – excited spectra (right) fitted with three Lorentzians to include the 2202 cm^{-1} bleach. Attempts to fit the spectra with Voigt functions resulted in a Lorentzian shapes with the Gaussian width vanishing.

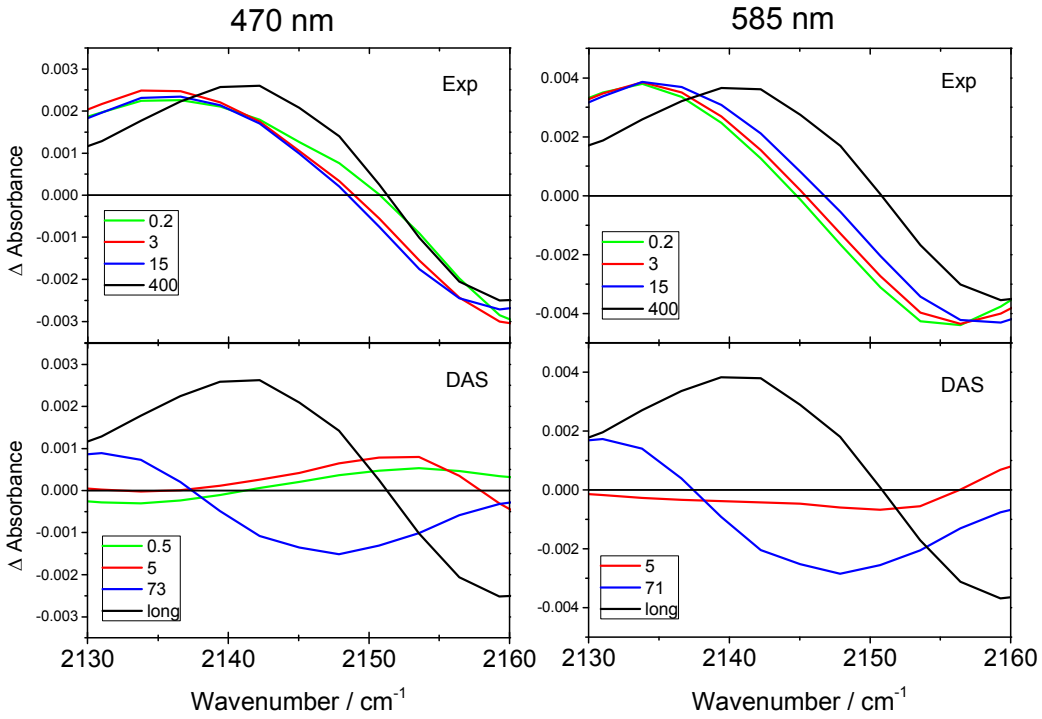

Figure S2. Time-evolution of IR spectra of Ir(dimen) in MeCN after 470 nm (left) and 585 nm (right) excitation measured with a magic angle between Vis pump and IR probe polarizations. Detail of the 2130-2160 cm^{-1} region. Top: Difference TRIR spectra measured at selected time delays. Bottom: decay associated spectra obtained by multiexponential global fitting.

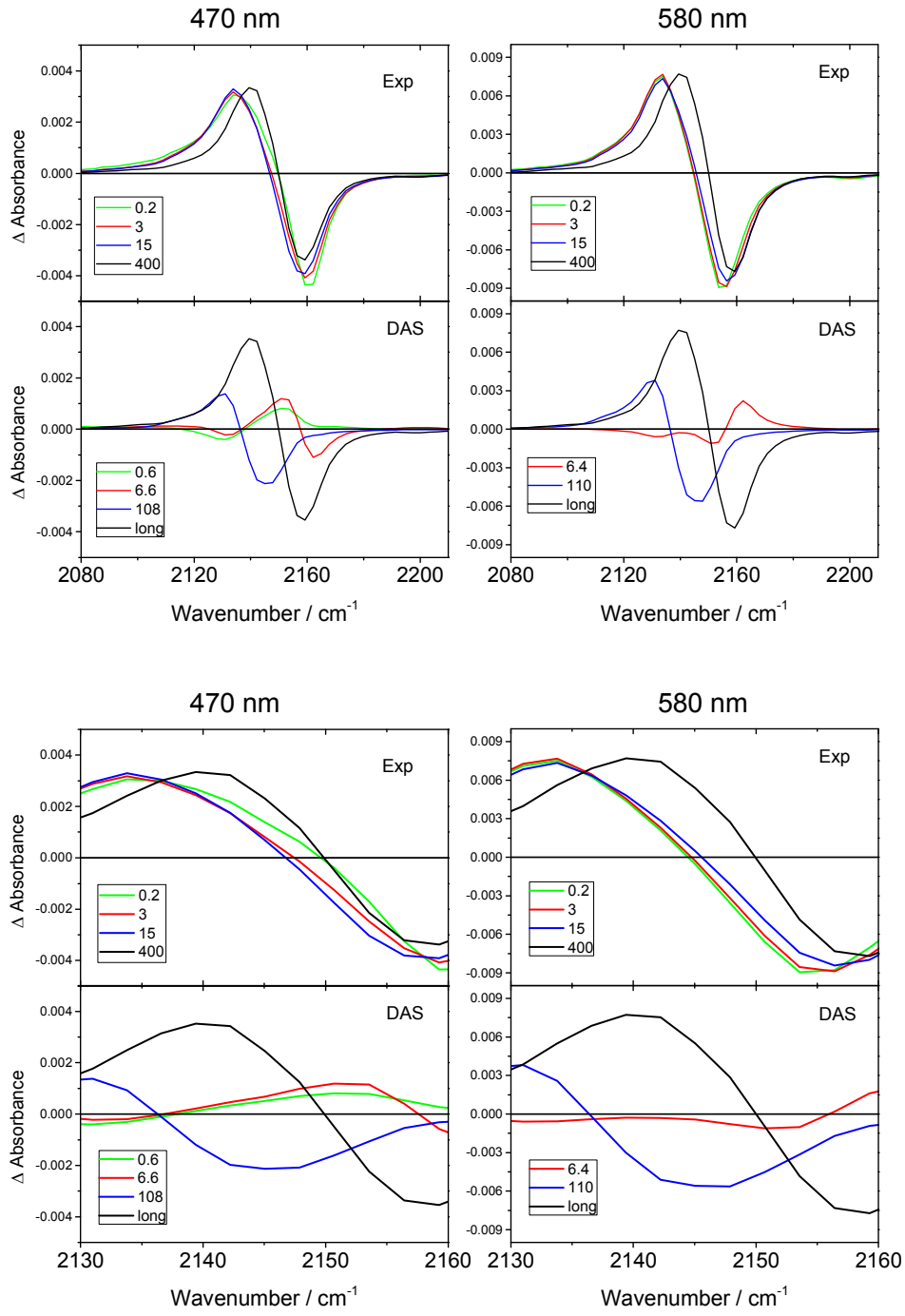

Figure S3. Time-evolution of IR spectra of Ir(dimen) in DCM after 470 nm (left) and 585 nm (right) excitation measured with a magic angle between Vis pump and IR probe polarizations. Top: Difference TRIR spectra measured at selected time delays. Bottom: decay associated spectra obtained by multiexponential global fitting. The lower panel shows the detail of the 2130-2160 cm^{-1} region.

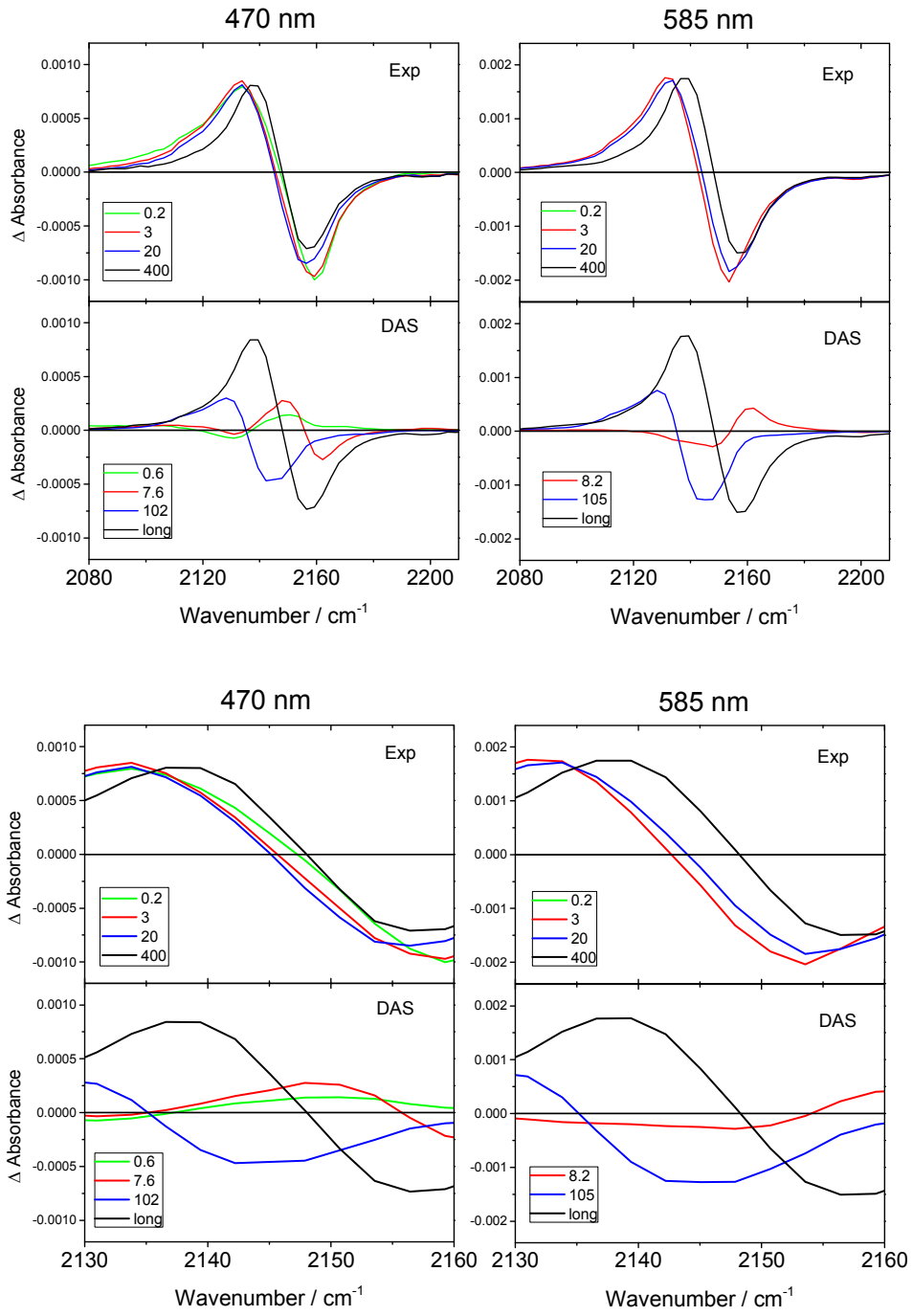

Figure S4. Time-evolution of IR spectra of Ir(dimen) in THF after 470 nm (left) and 585 nm (right) excitation measured with a magic angle between Vis pump and IR probe polarizations. Top: Difference TRIR spectra measured at selected time delays. Bottom: decay associated spectra obtained by multiexponential global fitting. The lower panel shows the detail of the 2130-2160 cm^{-1} region.

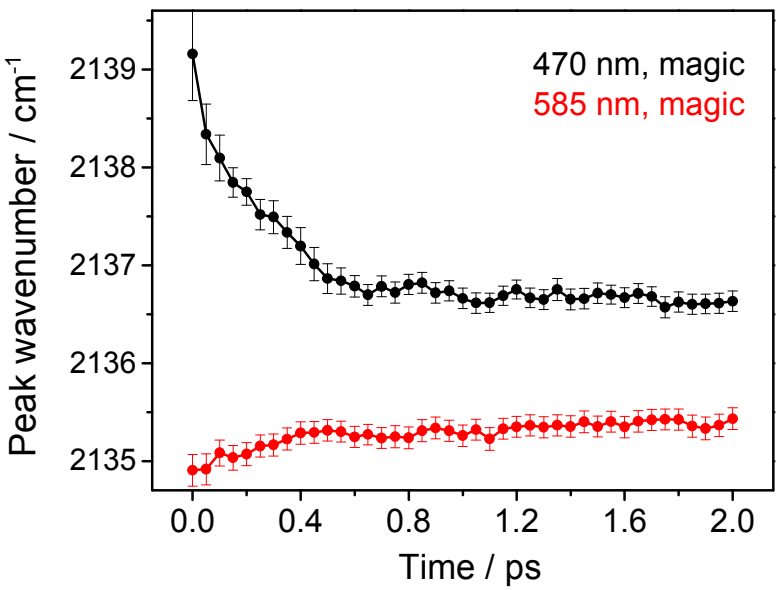

Figure S5. Time dependences of the maximum wavenumber of the transient IR band of Ir(dimen) in MeCN after 470 and 585 nm excitation at a magic angle polarization.

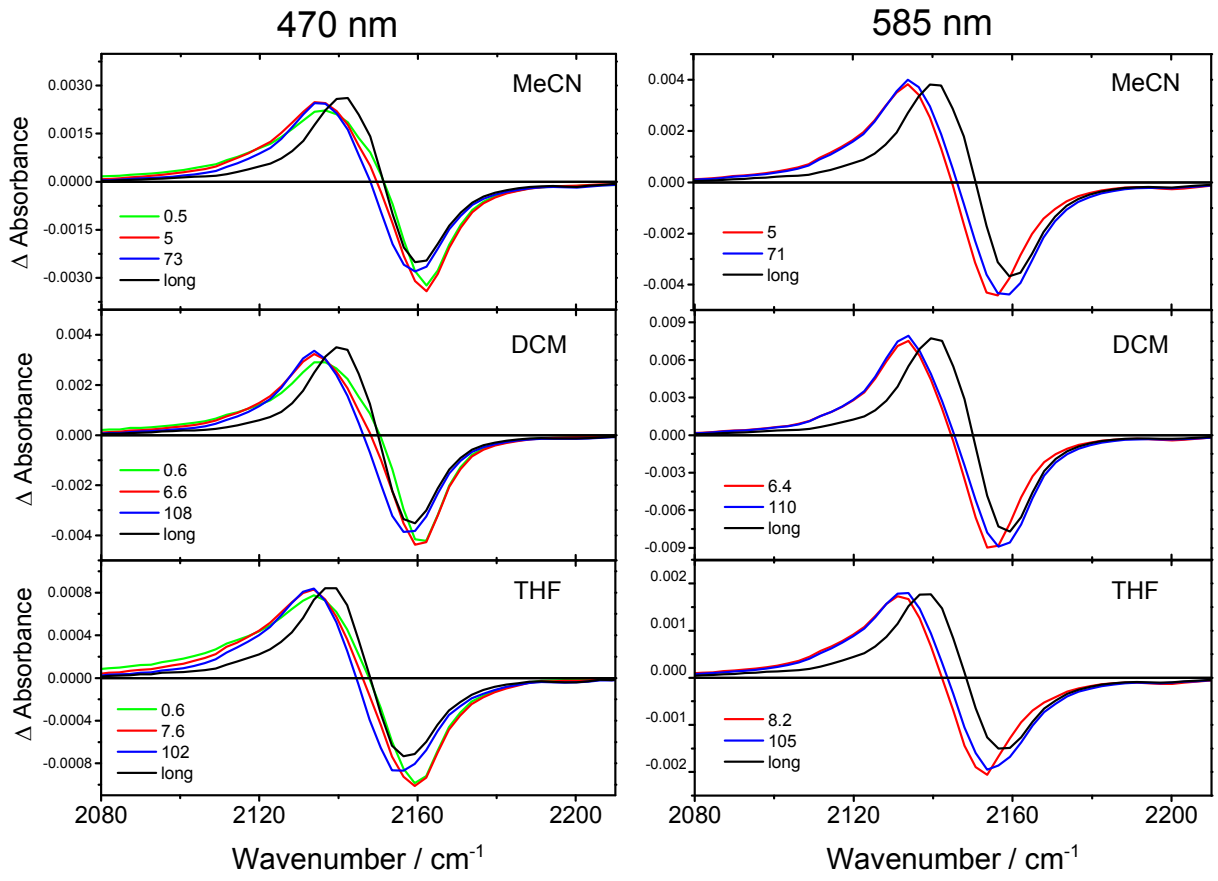

Figure S6. Difference evolution associated (EA) spectra obtained by multiexponential global fitting of Ir(dimen) TRIR spectra in MeCN, DCM, and THF measured upon 470 nm (left) and 585 nm (right) excitation with a magic angle between Vis pump and IR probe polarizations. EA spectra can be approximately regarded as difference IR spectra at the beginning of the associated kinetics step.

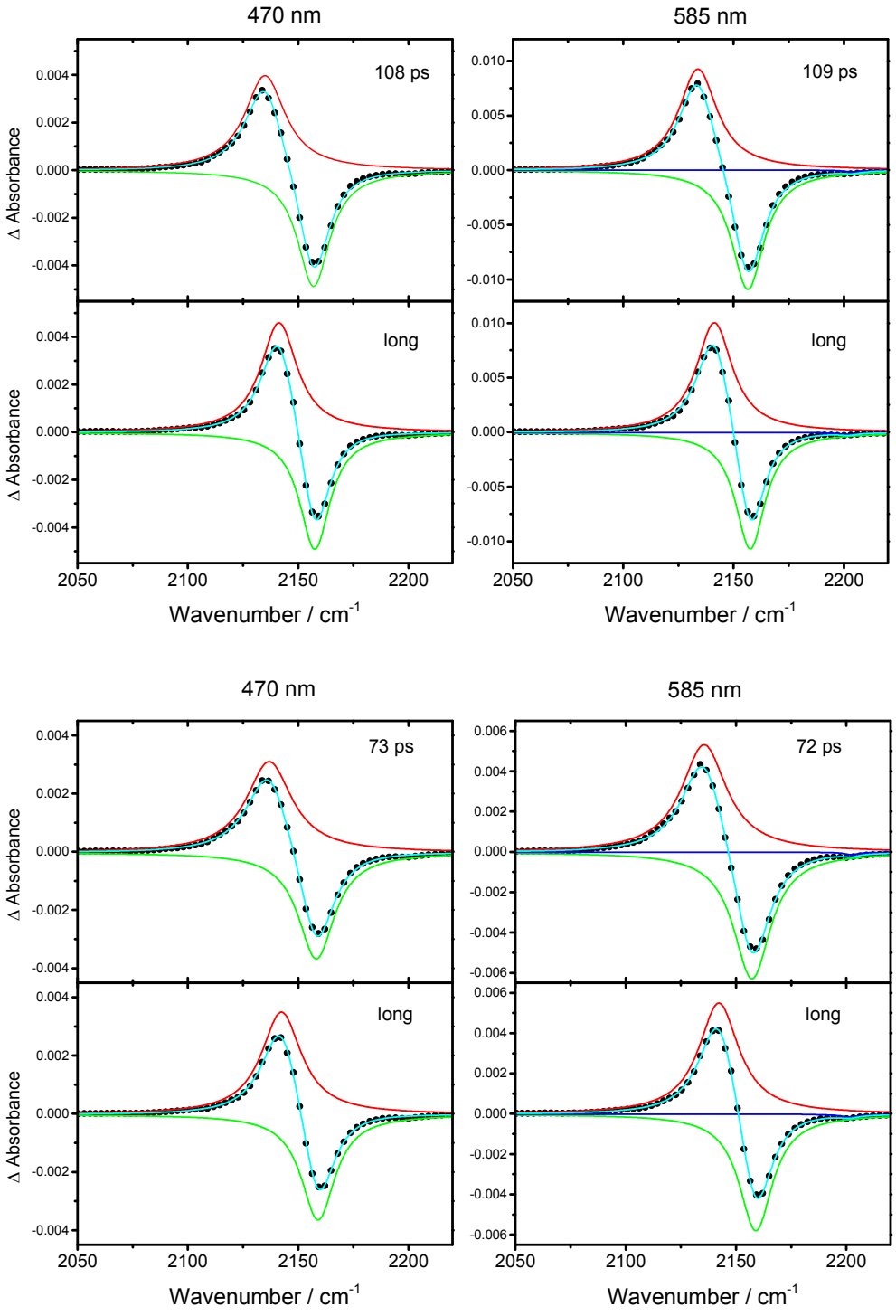

Figure S7. Representative Lorentzian fits of ISC and "long" EA spectra to determine positions and widths of ν(C≡N) IR bands of Ir(dimen) ^{1}dσ*pσ and ^{3}dσ*pσ excited states, respectively. Top: in DCM. Bottom: in MeCN. 470 nm – excited spectra (left) fitted with two Lorentzians, 585 nm – excited spectra (right) fitted with three Lorentzians to include the 2202 cm^{-1} bleach.

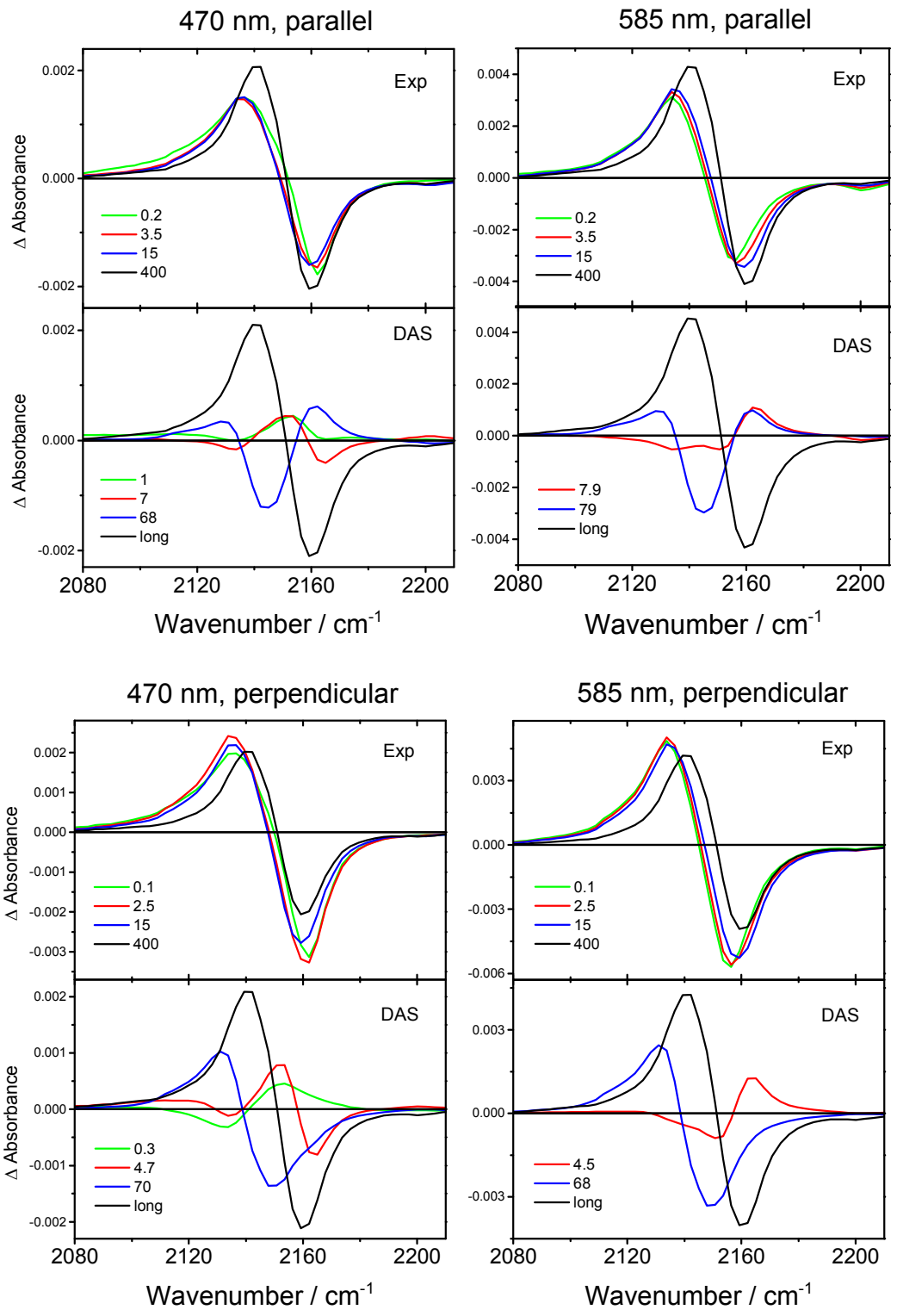

Figure S8. Time-evolution of IR spectra of Ir(dimen) in MeCN after 470 nm (left) and 585 nm excitation (right) obtained with parallel (top) and perpendicular (bottom) orientations of pump and probe polarization directions.

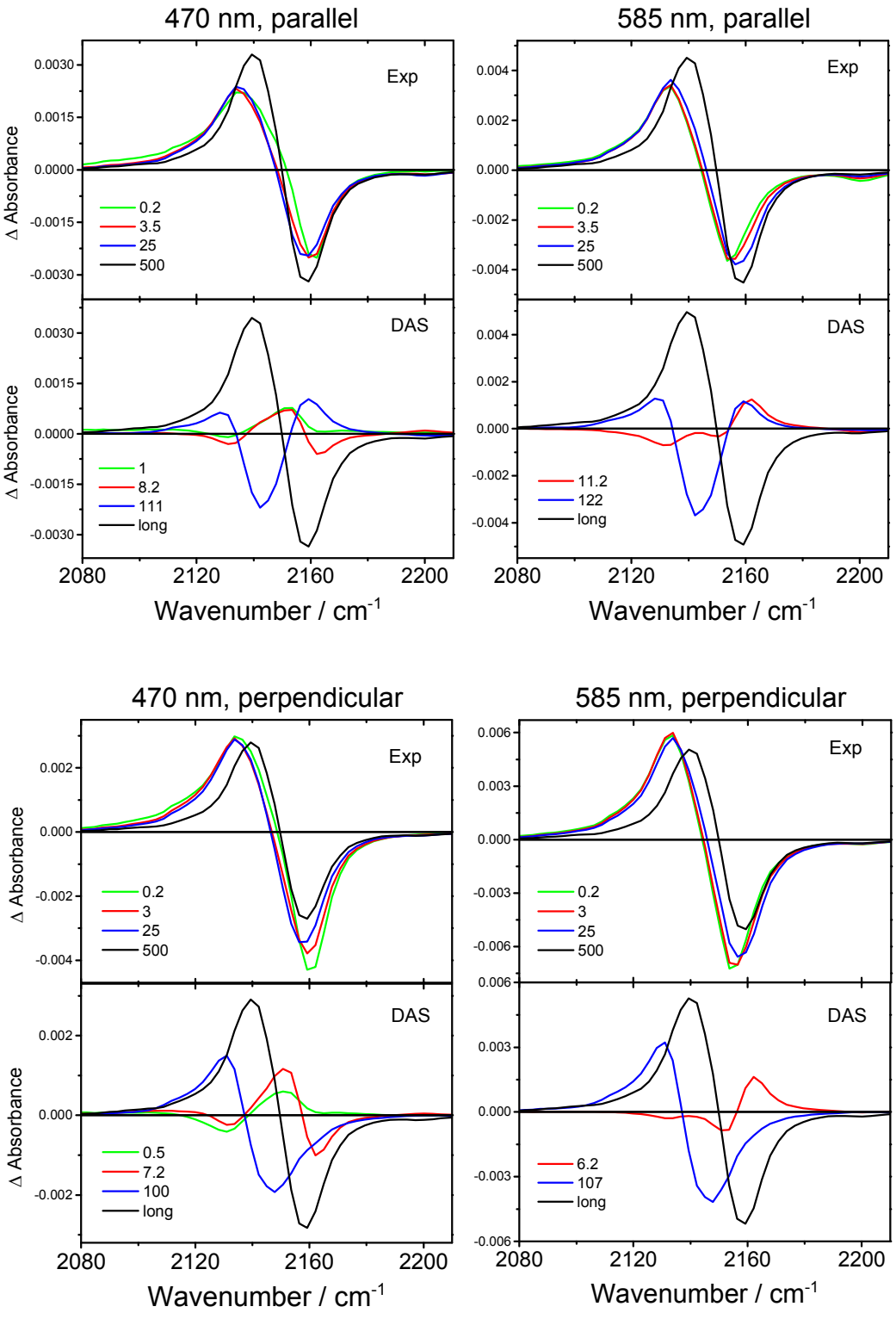

Figure S9. Time-evolution of IR spectra of Ir(dimen) in DCM after 470 nm (left) and 585 nm excitation (right) obtained with parallel (top) and perpendicular (bottom) orientations of pump and probe polarization directions.

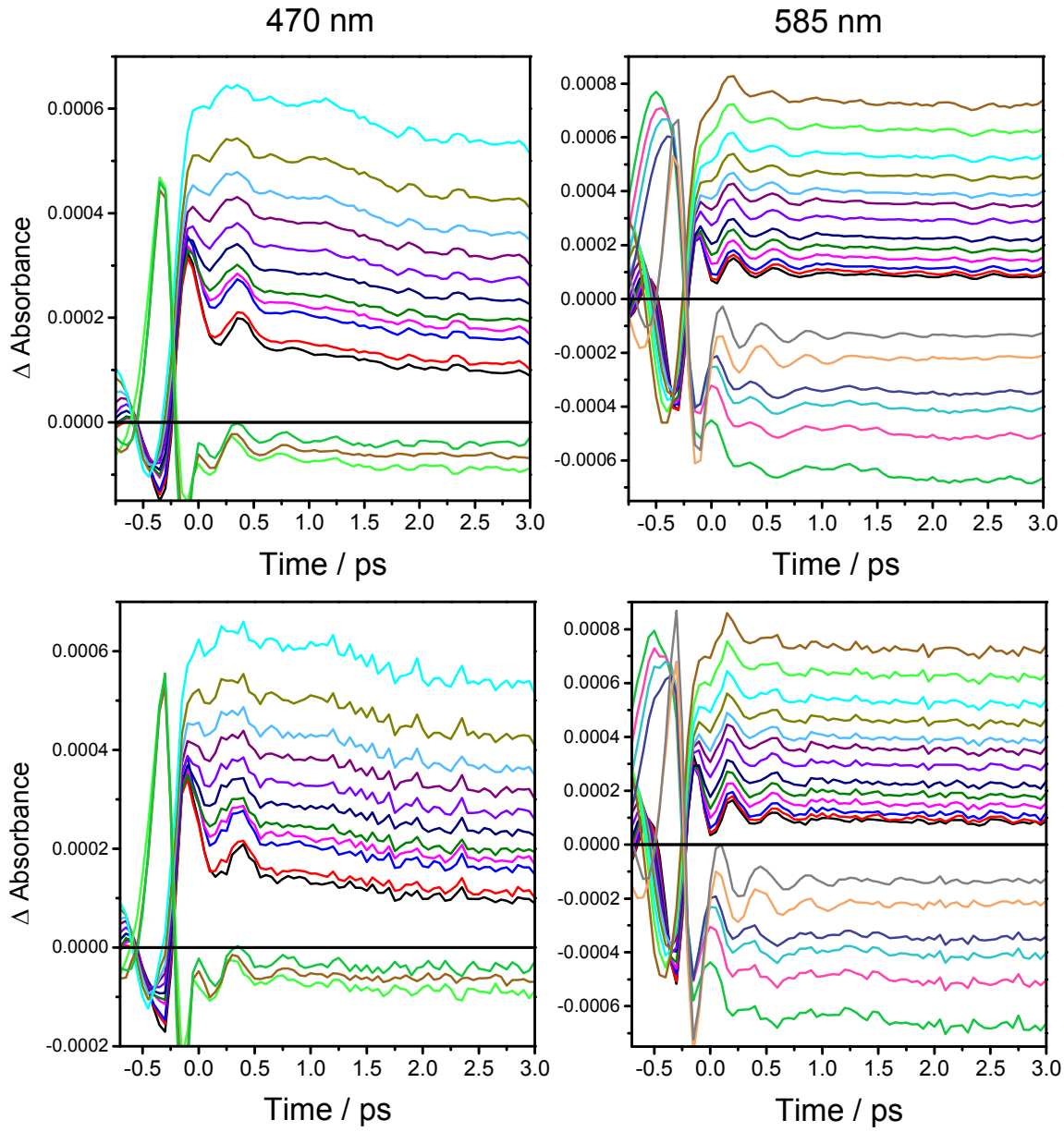

Figure S10a. Selected kinetics traces of Ir(dimen) in DCM measured after 470 nm and 585 nm excitation with magic angle between pump and probe beam polarizations. Top: 3-point averaging applied. Bottom: raw data. Traces in the left panel were measured at (from top down): 2109, 2106, 2103, 2101, 2098, 2095, 2093, 2090, 2087, 2085, 2082 cm^{-1}, break line, 2221, 2215, 2206 cm^{-1}. Right panel: 2103, 2101, 2098, 2095, 2093, 2090, 2087, 2085, 2082, 2079, 2077, 2074, 2071 cm^{-1}, break line, 2215, 2209, 2188, 2185, 2182, 2180 cm^{-1}.

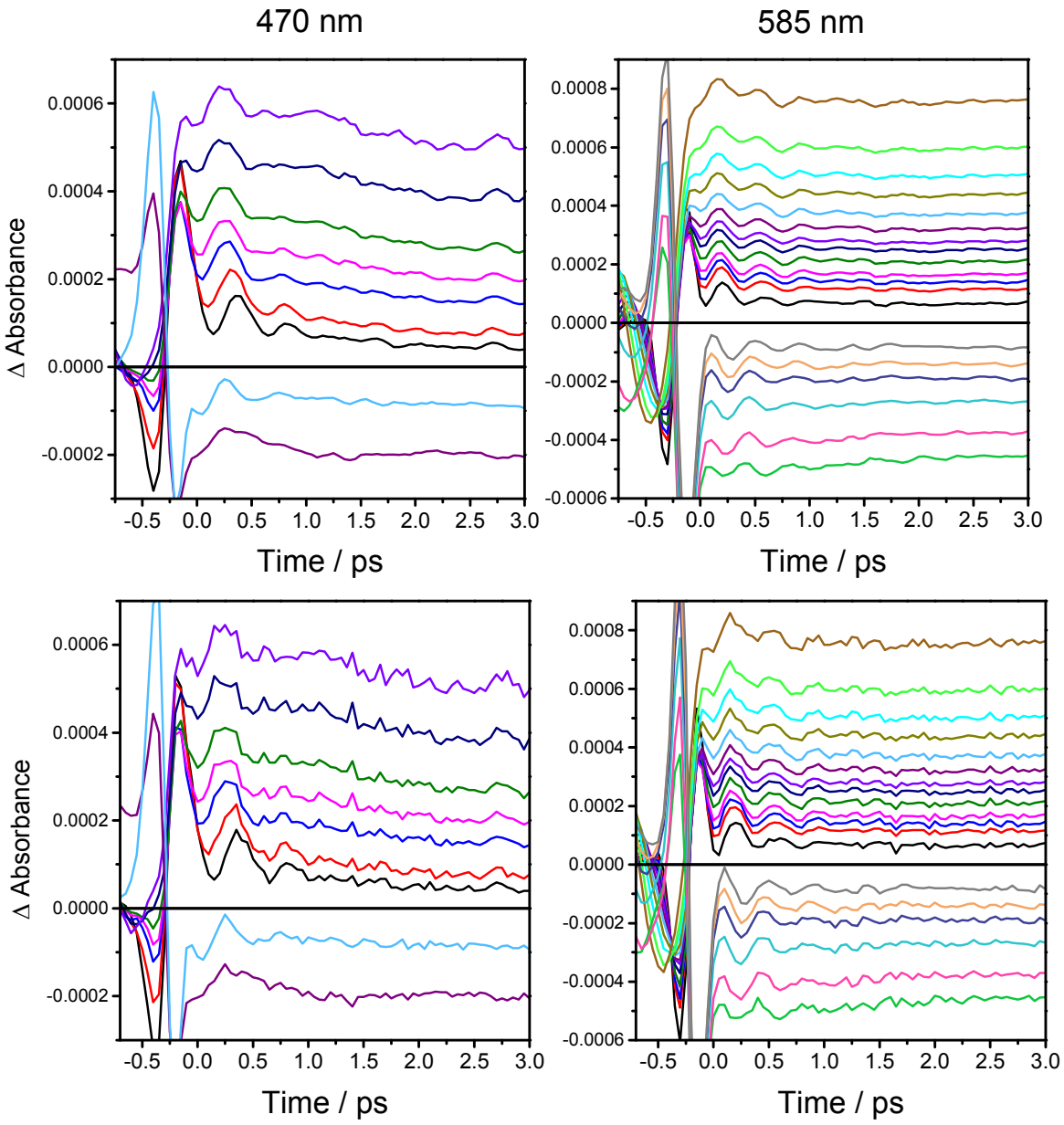

Figure S10b. Selected kinetics traces of Ir(dimen) in DCM measured after 470 nm and 585 nm excitation with parallel pump and probe beam polarizations. Top: 3-point averaging applied. Bottom: raw data. Traces in the left panel were measured at (from top down): 2112, 2109, 2104, 2098, 2093, 2082, 2071 cm^{-1}, break line, 2209, 2182 cm^{-1}. Right panel: 2109, 2106, 2104, 2101, 2098, 2095, 2093, 2090, 2087, 2085, 2082, 2079, 2069 cm^{-1}, break line, 2221, 2215, 2212, 2209, 2206, 2197 cm^{-1}.

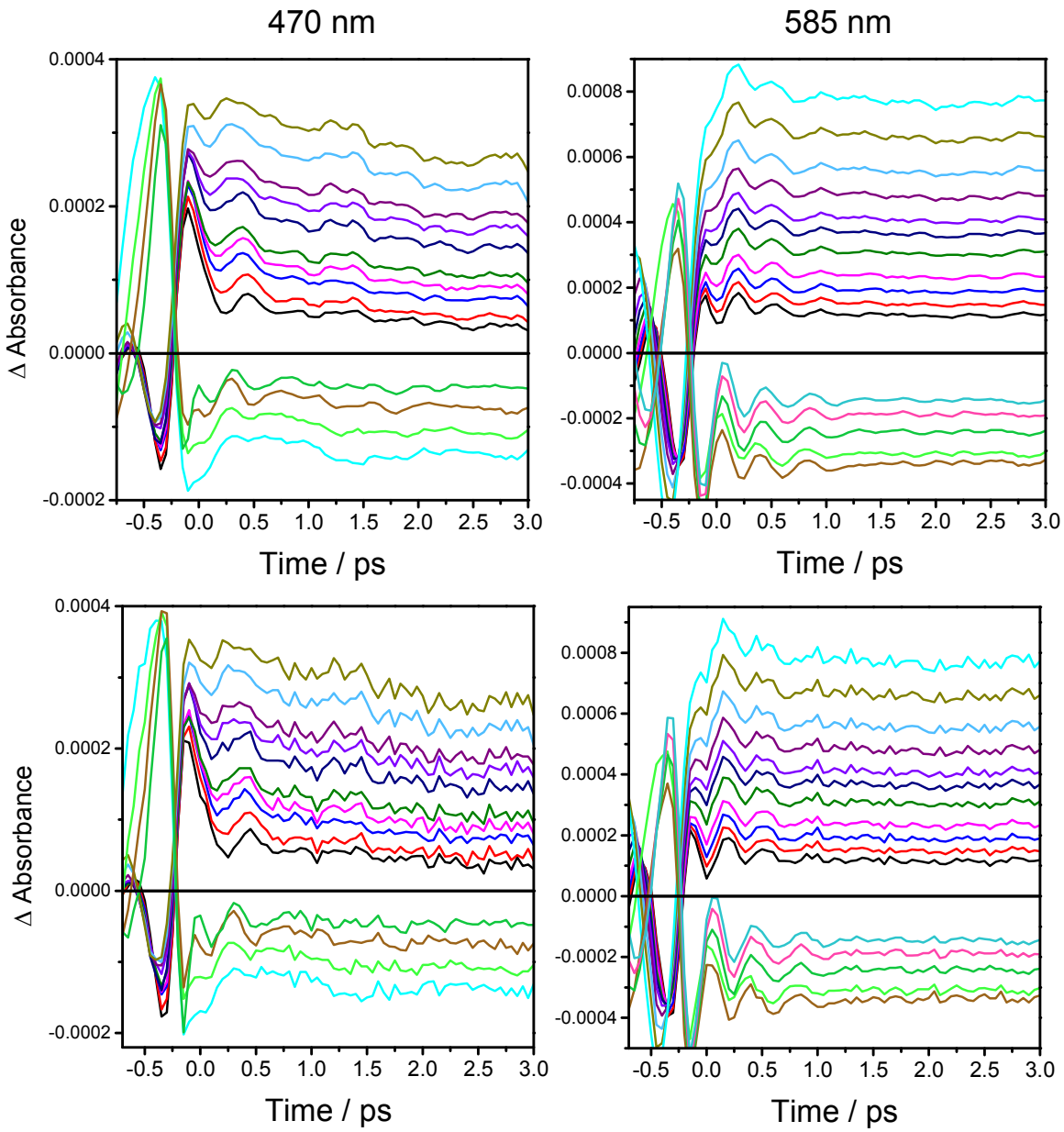

Figure S10c. Selected kinetics traces of Ir(dimen) in DCM measured after 470 nm and 585 nm excitation with perpendicular pump and probe beam polarizations. Top: 3-point averaging applied. Bottom: raw data. Traces in the left panel were measured at (from top down): 2098, 2095, 2093, 2090, 2087, 2085, 2082, 2079, 2074, 2063 cm^{-1}, break line, 2215, 2203, 2197, 2191 cm^{-1}. Right panel: 2104, 2101, 2098, 2095, 2093, 2090, 2087, 2085, 2082, 2079, 2077 cm^{-1}, break line, 2212, 2209, 2206, 2200, 2194 cm^{-1}.

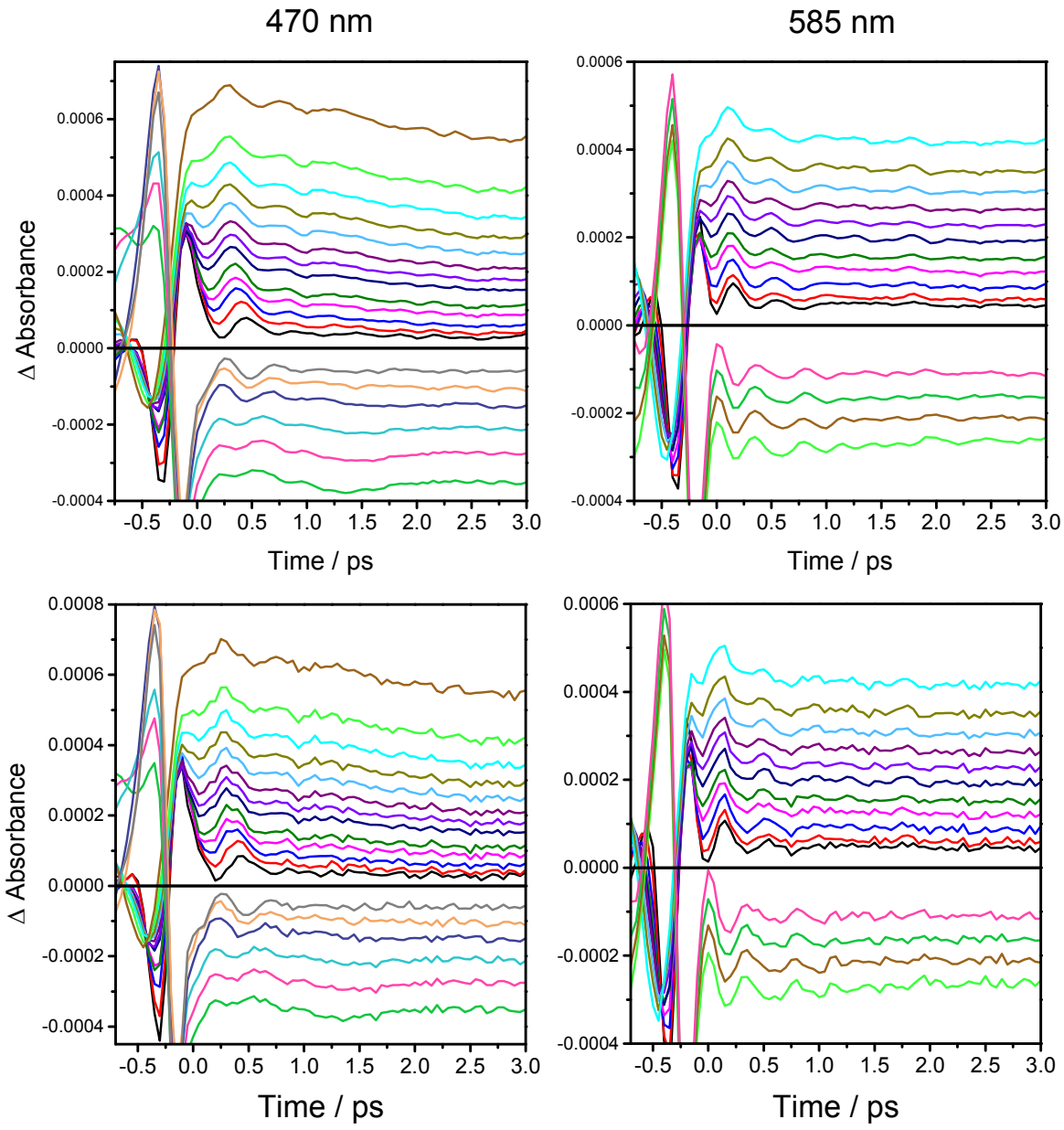

Figure S11a. Selected kinetics traces of Ir(dimen) in MeCN measured after 470 nm and 585 nm excitation with magic angle between pump and probe beam polarizations. Top: 3-point averaging applied. Bottom: raw data. Traces in the left panel were measured at (from top down): 2112, 2109, 2106, 2103, 2101, 2098, 2095, 2093, 2087, 2085, 2079, 2071, 2058 cm^{-1}, break line, 2218, 2206, 2200, 2188, 2185, 2182 cm^{-1}. Right panel: 2101, 2098, 2095, 2093, 2090, 2087, 2085, 2082, 2077, 2069, 2058 cm^{-1}, break line, 2215, 2209, 2206, 2203 cm^{-1}.

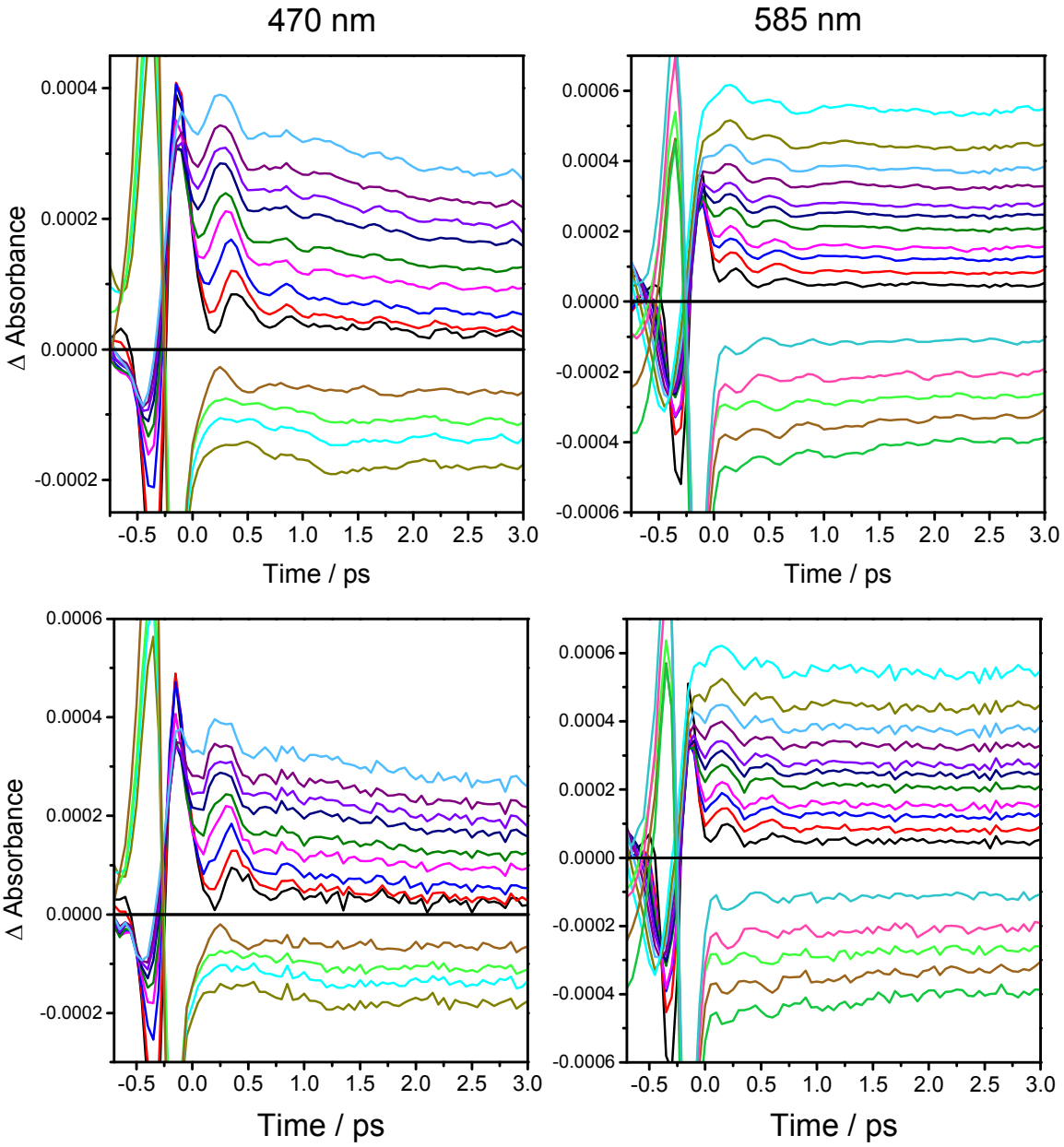

Figure S11b. Selected kinetics traces of Ir(dimen) in MeCN measured after 470 nm and 585 nm excitation with parallel pump and probe beam polarizations. Top: 3-point averaging applied. Bottom: raw data. Traces in the left panel were measured at (from top down): 2109, 2106, 2103, 2101, 2095, 2090, 2082, 2071, 2061 cm^{-1}, break line, 2209, 2188, 2185, 2182 cm^{-1}. Right panel: 2109, 2106, 2103, 2101, 2098, 2095, 2093, 2087, 2085, 2079, 2063 cm^{-1}, break line, 2215, 2209, 2200, 2197, 2194 cm^{-1}.

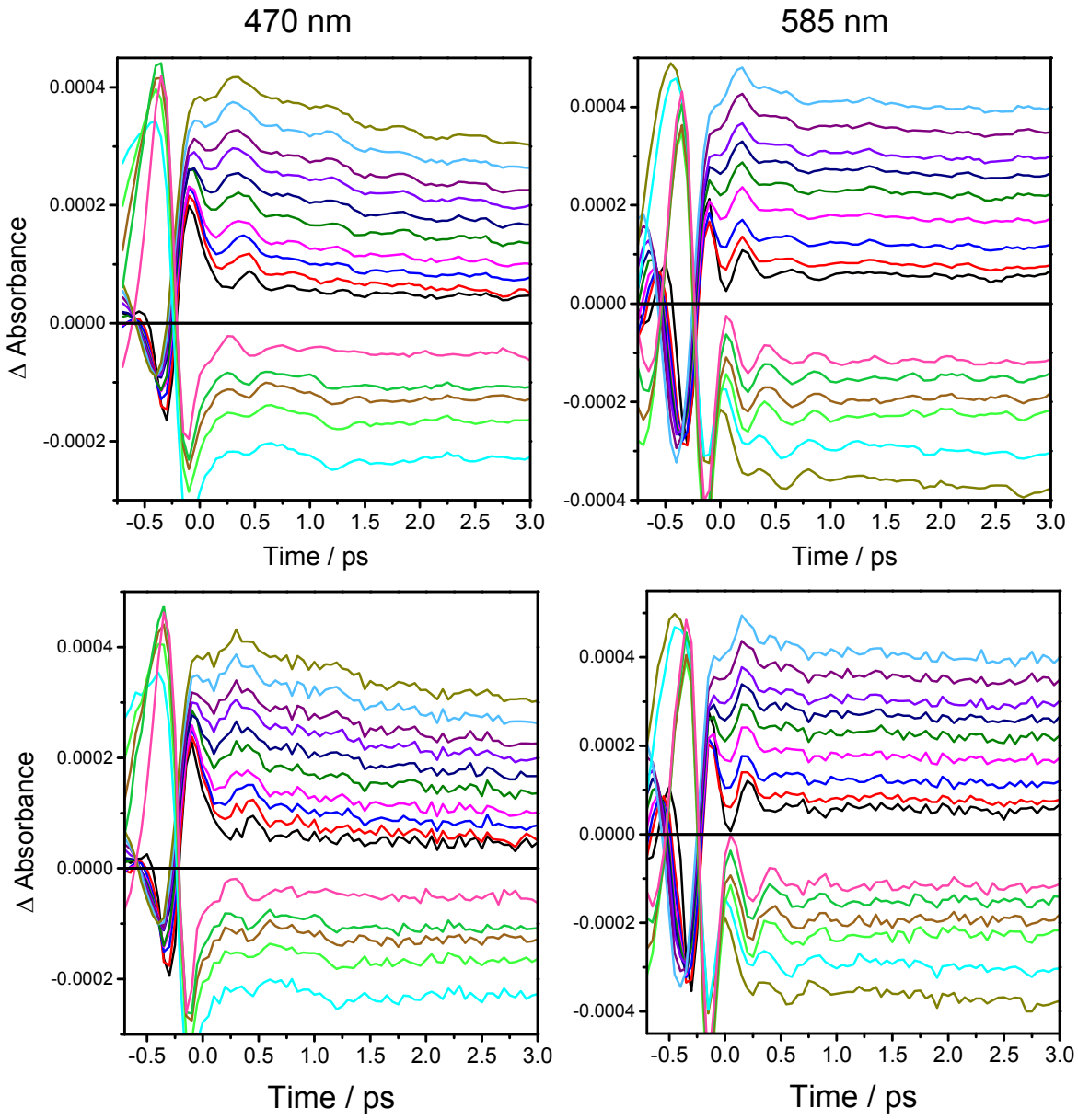

Figure S11c. Selected kinetics traces of Ir(dimen) in MeCN measured after 470 nm and 585 nm excitation with perpendicular pump and probe beam polarizations. Top: 3-point averaging applied. Bottom: raw data. Traces in the left panel were measured at (from top down): 2103, 2101, 2098, 2095, 2093, 2087, 2085, 2079, 2074, 2058 cm^{-1}, break line, 2209, 2194, 2191, 2188, 2185, cm^{-1}. Right panel: 2098, 2095, 2093, 2090, 2087, 2085, 2079, 2074, 2058 cm^{-1}, break line, 2212, 2209, 2206, 2203, 2188, 2185 cm^{-1}.

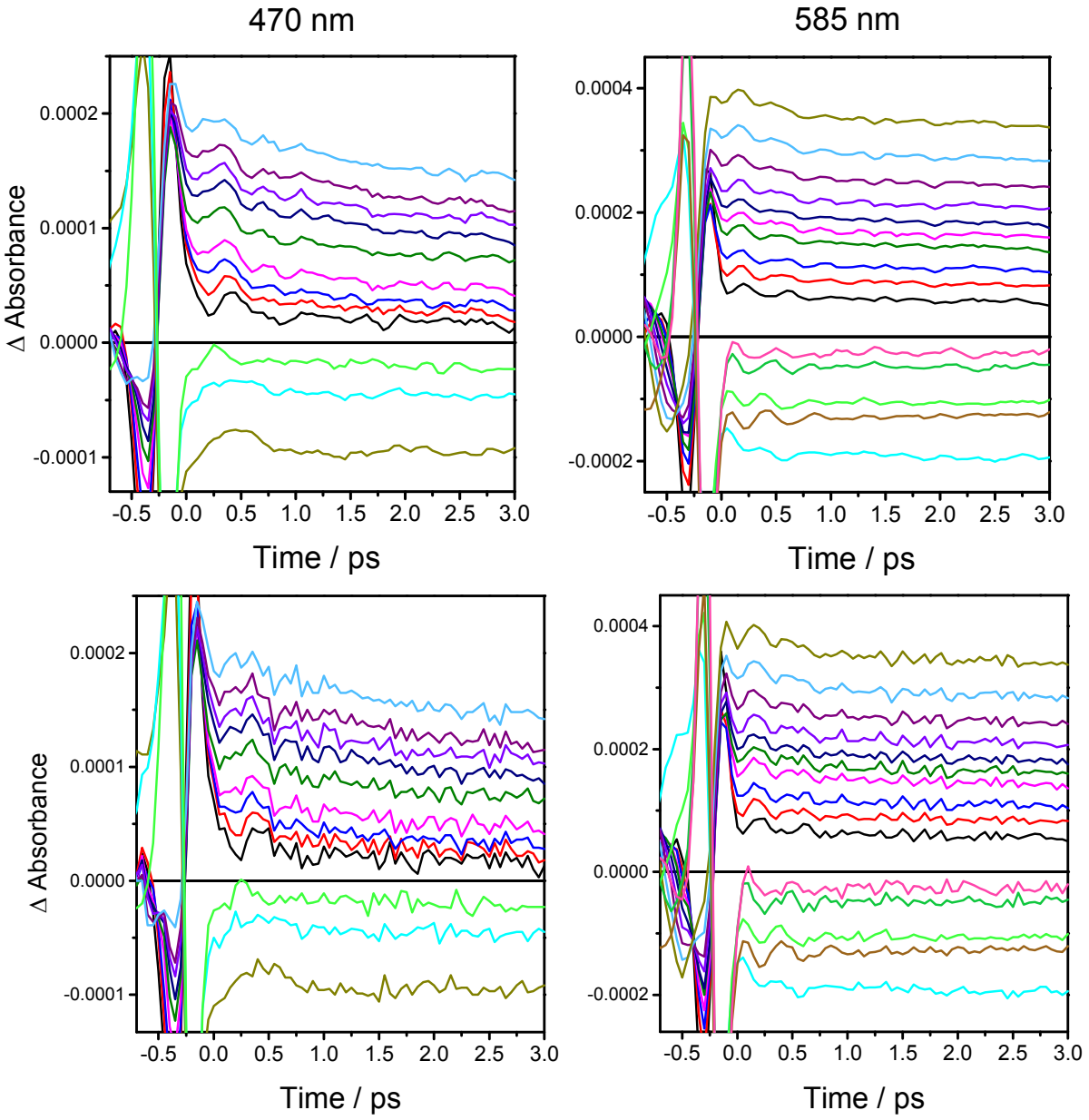

Figure S12. Selected kinetics traces of Ir(dimen) in THF measured after 470 nm and 585 nm excitation with magic angle between pump and probe beam polarizations. Bottom: raw data. Top: 3-point averaging applied. Traces in the left panel were measured at (from top down): 2103, 2101, 2098, 2095, 2093, 2085, 2079, 2069, 2058 cm^{-1}, break line, 2209, 2188, 2182 cm^{-1}. Right panel: 2106, 2103, 2101, 2098, 2095, 2093, 2090, 2085, 2079, 2063, break line, 2224, 2212, 2200, 2191, 2179 cm^{-1}.

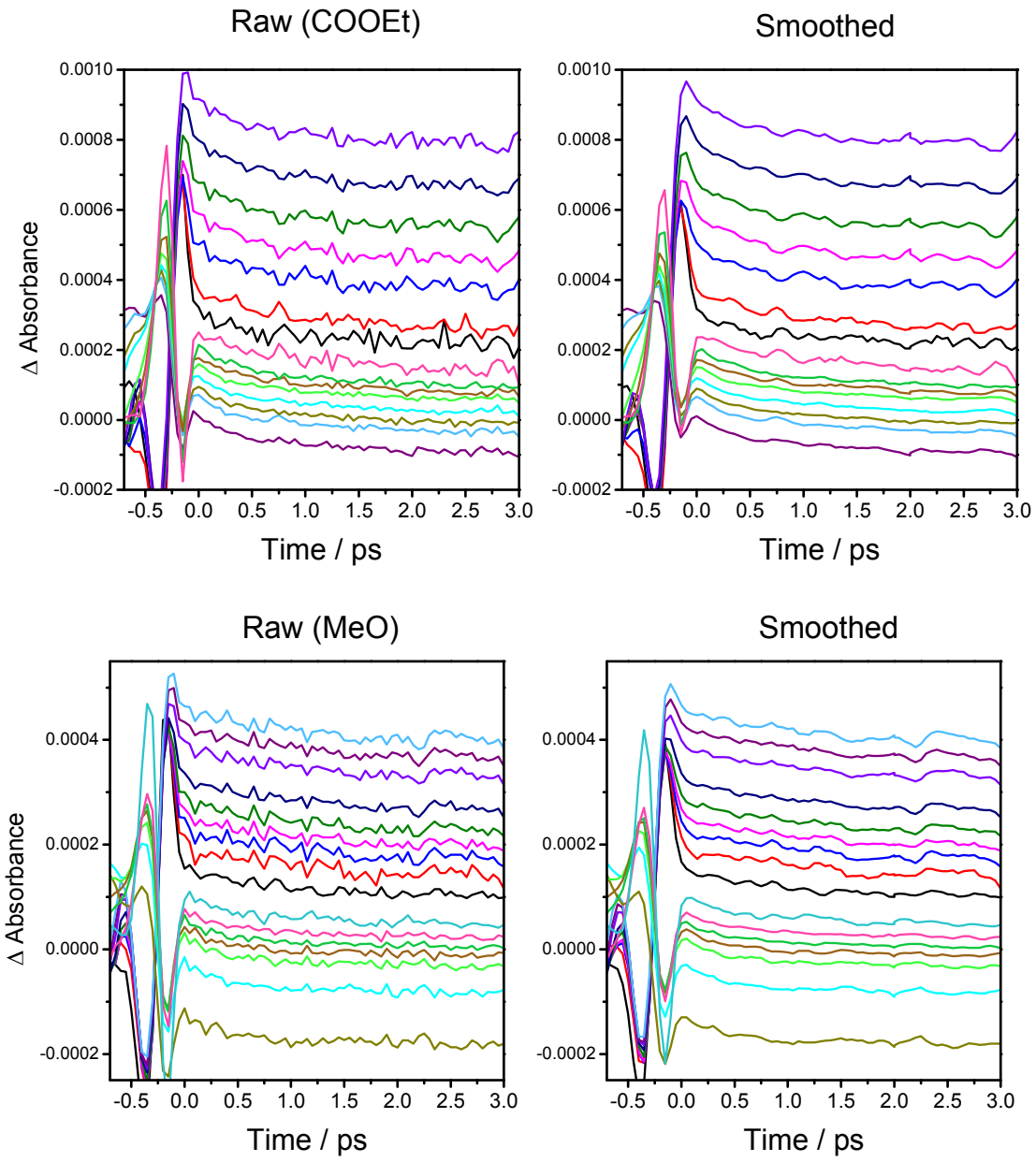

Figure S13. A control experiment: Kinetics traces measured at the low-and high-frequency sides of the ν(N=C) TRIR band of the ^{3}MLCT excited-state of [Ru(4,4'-(COOEt)$_2$-bpy)$_2$(NCS)$_2$] and [Ru(4,4'-(MeO)$_2$-bpy)$_2$(NCS)$_2$] in DMF after 470 nm excitation. Left: raw data. Right: 3-point adjacent averaging applied. Measurements were performed at identical experimental conditions (instrument settings, the cell, the day, etc.) as Ir(dimen) experiments. The absence of signal oscillations shows that they are compound-specific and not experimental artifacts. Accordingly, FFT analysis shows neither the 77-88 cm^{-1} peak nor any signs of periodicity superimposed on the kinetics traces. Detection wavelengths from top to bottom (COOEt): 2006, 2001, 1996, 1991, 1986, 1967, 1948, 2186, 2168, 2151, 2142, 2134, 2131, 2128, 2125 cm^{-1}; (MeO): 2021, 2019, 2016, 2011, 2006, 2001, 1996, 1986, 1974, 2168, 2142, 2131, 2128, 2125, 2123, 2120 cm^{-1}.

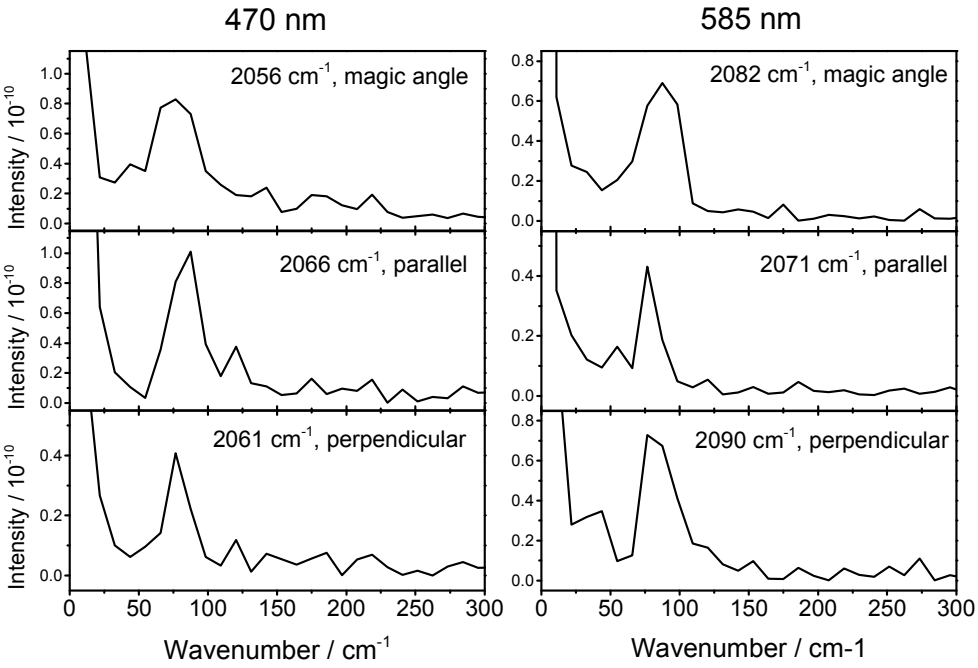

Figure S14. Fast Fourier transforms of selected kinetics traces measured in DCM. FFT was performed over the 0-2 ps range, data were acquired every 50 fs. FFT points are separated by ca. 11 cm^{-1}.

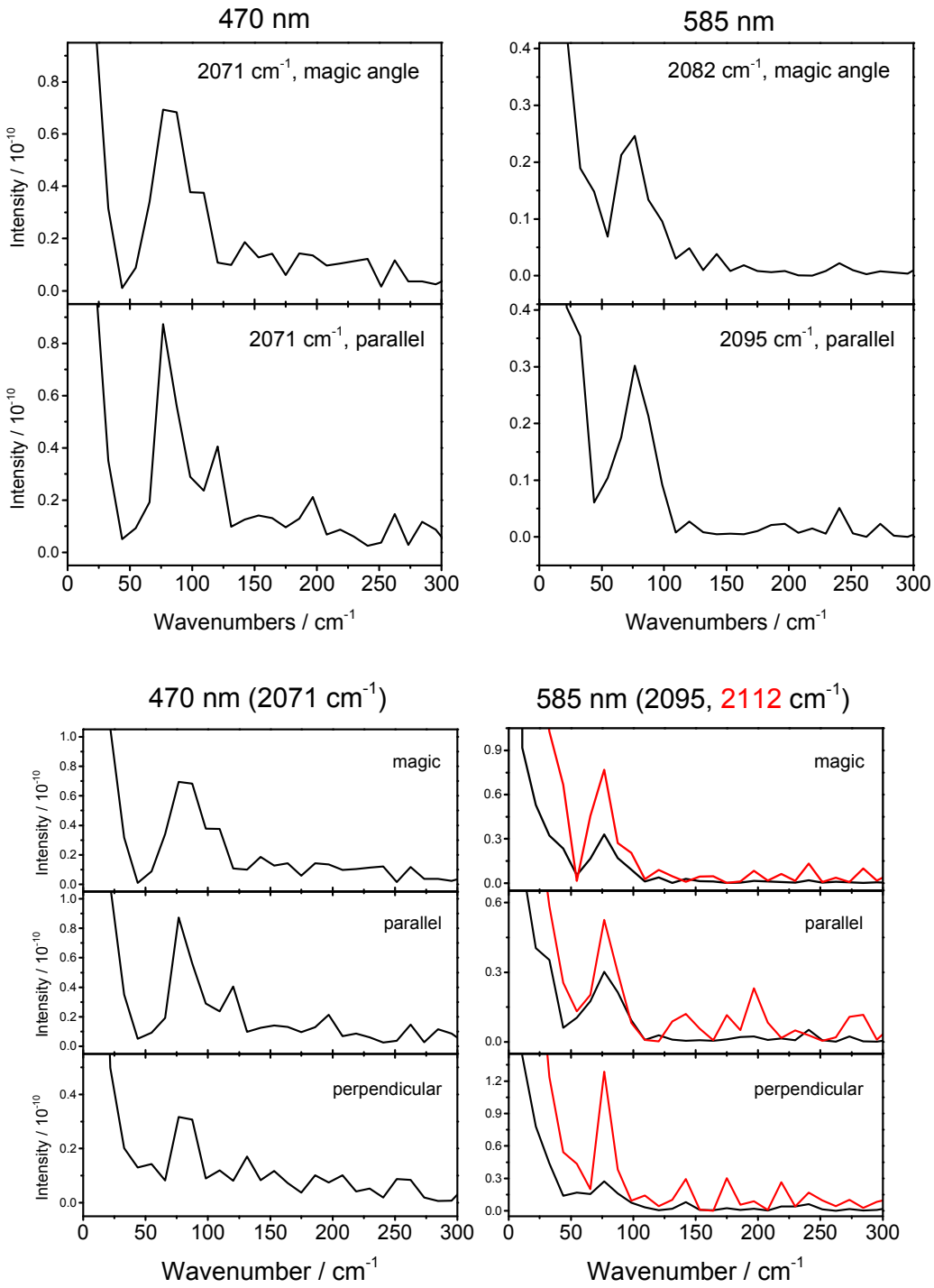

Figure S15. Fast Fourier transforms of selected kinetics traces measured in MeCN. FFT was performed over the 0-2 ps range, data were acquired every 50 fs. FFT points are separated by ca. 11 cm^{-1}. Note, that oscillations of the 2112 cm^{-1} traces are rather weak but the 77-88 cm^{-1} beat can still be identified.

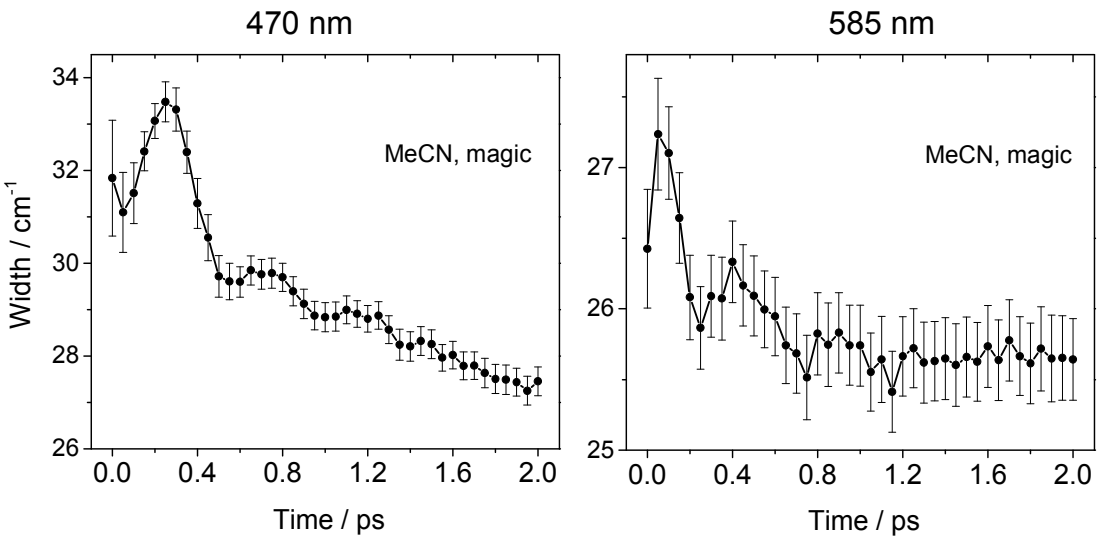

Figure S16. Time dependent width (FWHM) of the Ir(dimen) excited-state IR band measured after 470 (left) and 585 (right) nm excitation in MeCN at magic angle polarization.

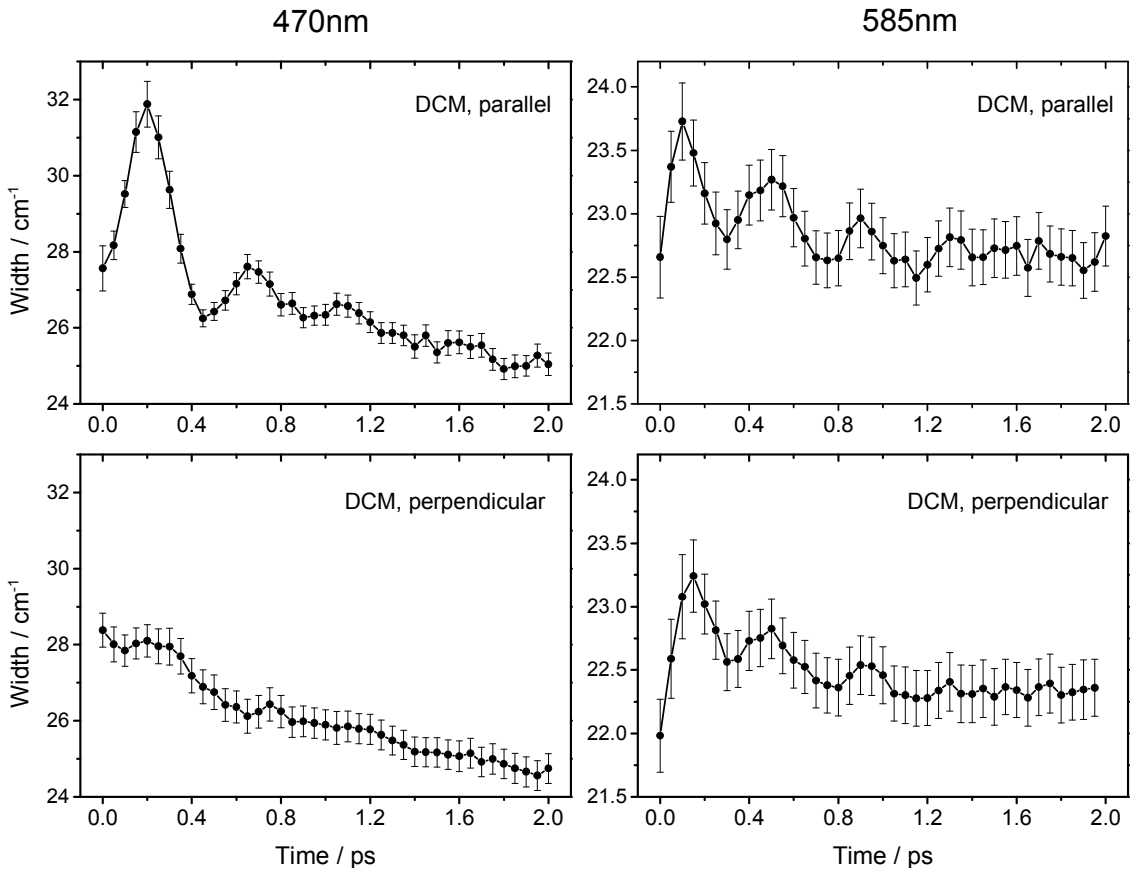

Figure S17. Time dependent width (FWHM) of the Ir(dimen) excited-state IR band measured after 470 (left) and 585 (right) nm excitation in DCM at parallel and perpendicular polarizations.

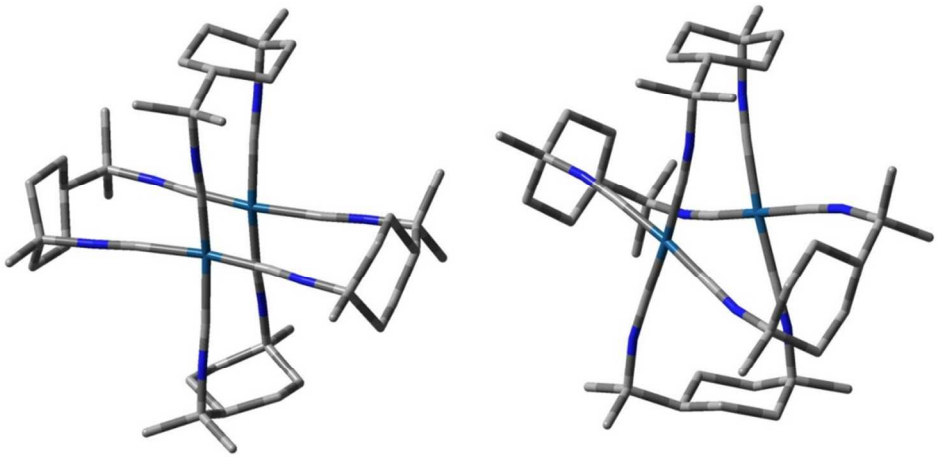

Figure S18. UKS-DFT optimized structures of the long/eclipsed (left) and short/twisted (right) isomers of Ir(dimen) in the triplet excited state. Hydrogen atoms omitted for simplicity. Comparison with Figure 1 reveals that, relative to the ground state, the Ir atoms are slightly displaced inwards from the facial planes. The structure on the right is visually undistinguishable from those of the lowest singlet excited state and the TDDFT triplet structure.

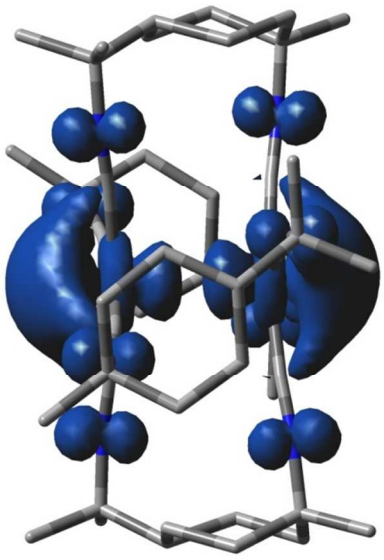

Figure S19. UKS-DFT calculated spin density distribution in the lowest triplet state ($^3B_1$) of Ir(dimen).

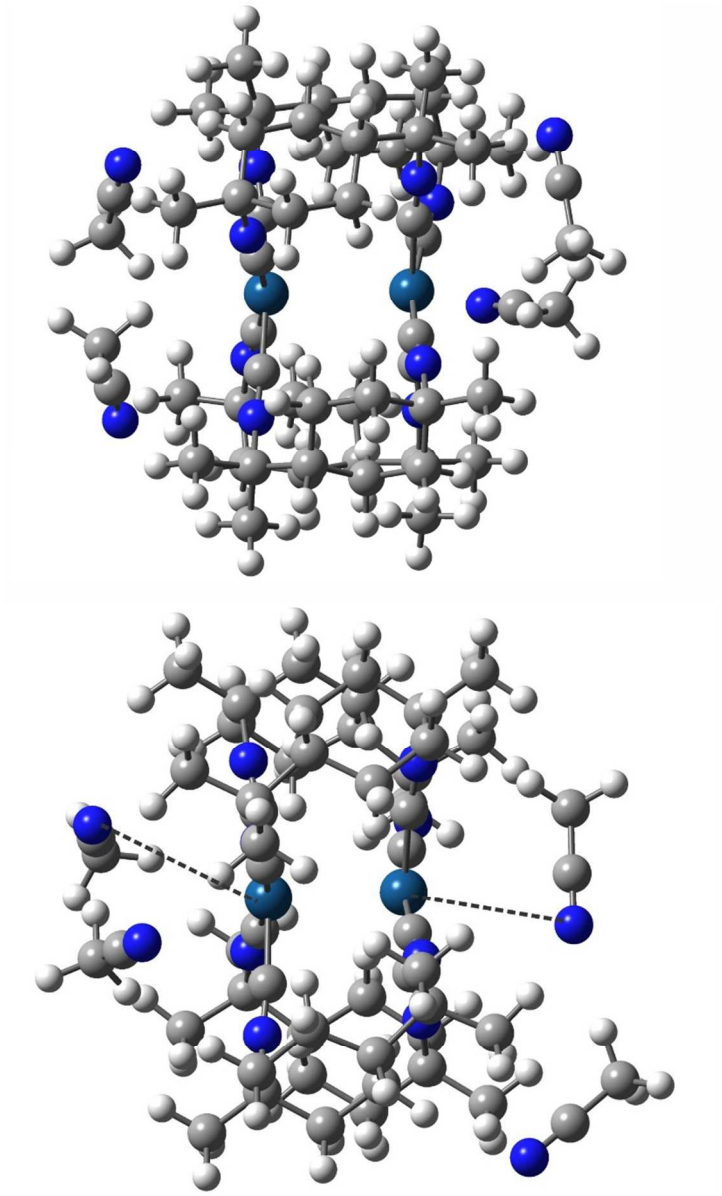

Figure S20. UKS-DFT optimized structures of the short/twisted isomer of Ir(dimen) with four MeCN molecules in the ground- (top) and lowest triplet (bottom) states. The whole Ir(dimen)·4MeCN cluster is embedded in a PCM-modelled implicit MeCN. Ground-state structure does not exhibit any preferential orientation of MeCN towards the Ir(dimen). The triplet structure shows that N atoms of close-lying MeCN molecules are oriented towards Ir. The dashed lines indicate the shortest calculated Ir–N(MeCN) distances of 3.86 and 4.09 Å.

TABLES

Table S1. TDDFT-calculated ν(C≡N) wavenumbers (cm^{-1}) and intensities (in parenthesis, 10^3 km/mol) of the ground state (a^1A) and lowest excited singlet (b^1B_1) and triplet (a^3B_1) states of the short/twisted isomer of Ir(dimen) in MeCN, assuming D_2 symmetry. Wavenumbers are scaled by 0.956.

a^1A	Exp.	a^1B_1	Exp-a^1B_1	a^3B_1	Exp-a^3B_1
2147 (0.0); B_2	2128	2139(0.0); B_3		2136(4.3); B_1	
2147 (0.0); B_3		2139(0.0); A		2139(0.0); B_3	
2153 (5.7); B_2	2158	2140(0.7); B_2		2139(0.5); B_2	
2153 (5.9); B_3		2142(0.0); B_1		2140(0.0); A	
2170 (0.0); A		2143(5.2); B_2	2136	2143(0.0); B_1	
2172 (0.0); B_1		2143(6.2); B_3		2143(5.5); B_2	2142
2212 (0.5); B_1	2200	2185(0.1); B_1		2143(6.3); B_3	
2231 (0.0); A		2219(0.0); A		2222(0.0); A	

Table S2. UKS-DFT-calculated and experimental vibrations of the Ir(dimen) ground state and $^3d\sigma^*p\sigma$ lowest triplet. In MeCN, no symmetry assumed.

short/twisted	long/eclipsed		twisted	eclipsed	
GS	GS	Exp.	$^3d\sigma^*p\sigma$	$^3d\sigma^*p\sigma$	Exp.
2147 (0.0)	2164 (0.2)	2128	2137(0.0)	2143(0.0)	
2147 (0.0)	2164 (0.0)		2137(1.3)	2143(0.0)	
2153 (5.7)	2168 (6.0)	2158	2138(0.0)	2145(0.0)	
2153 (5.9)	2168 (5.9)		2141(0.0)	2145(0.0)	
2170 (0.0)	2188 (0.0)		2141(4.8)	2147(6.3)	2142
2172 (0.0)	2190 (0.0)		2141(6.4)	2147(6.3)	
2212 (0.5)	2240 (0.0)	2200	2153(2.2)	2155(3.5)	
2231 (0.0)	2243 (0.0)		2222(0.0)	2227(0.0)	

Table S3. DFT-calculated one-electron energies and compositions of selected frontier molecular orbitals of the ground-state short/twisted deformational isomer of Ir(dimen). (PBE0/GD3/PCM-MeCN, no symmetry assumed)

MO	E (eV)	Prevailing character	Ir	C(C≡N)	N
Unoccupied					
LUMO+2	-0.57	CN(π*)	7	55	28
LUMO+1	-0.94	Ir (pσ*)+CN(π*)	23	46	24
LUMO	-2.74	Ir (pσ)+CN(π*)	34	34	27
Occupied					
HOMO	-5.79	Ir (dσ*)	88	8	3
HOMO-1	-7.12	Ir (dπ*)	75	3	16
HOMO-2	-7.13	Ir (dπ*)	75	3	16
HOMO-3	-7.61	Ir (dπ)	69	2	21
HOMO-4	-7.62	Ir (dπ)	69	3	21
HOMO-5	-7.73	Ir (dσ)	98	1	0
HOMO-6	-7.90	Ir (dπ)	49	3	28
HOMO-7	-7.93	Ir (dπ)	53	3	30

Table S4. DFT-calculated one-electron energies and compositions of selected frontier molecular orbitals of Ir(dimen) at the TDDFT optimized geometry of the lowest excited singlet state. (PBE0/GD3/PCM-MeCN, D_2 symmetry assumed.)

MO	E (eV)	Prevailing character	Ir	C(C≡N)	N
Unoccupied					
LUMO+2	-0.62	CN(π*)	12	55	27
LUMO+1	-0.67	Ir (pσ*)+CN(π*)	11	46	28
LUMO	-2.82	Ir (pσ)+CN(π*)	29	34	29
Occupied					
HOMO	-5.46	Ir (dσ*)	84	9	5
HOMO-1	-6.93	Ir (dπ*)	77	4	15
HOMO-2	-6.93	Ir (dπ*)	77	4	15
HOMO-3	-7.89	Ir (dπ)	66	2	23
HOMO-4	-7.9	Ir (dπ)	66	2	23
HOMO-5	-7.91	Ir (dπ)	49	3	28
HOMO-6	-7.94	Ir (dπ)	53	3	30
HOMO-7	-8.42	Ir (dσ)	94	5	0

Table S5. DFT-calculated one-electron energies and compositions of selected frontier molecular orbitals of Ir(dimen) at the TDDFT* optimized geometry of the lowest triplet state (a^3B_1). (PBE0/GD3/PCM-MeCN, D_2 symmetry assumed.)

MO	E (eV)	Prevailing character	Ir	C(C≡N)	N
Unoccupied					
LUMO+2	-0.63	CN(π*)	12	50	27
LUMO+1	-0.68	Ir (pσ*)+CN(π*)	11	51	28
LUMO	-2.83	Ir (pσ)+CN(π*)	28	37	29
Occupied					
HOMO	-5.41	Ir (dσ*)	84	10	6
HOMO-1	-6.92	Ir (dπ*)	77	4	15
HOMO-2	-6.92	Ir (dπ*)	77	4	15
HOMO-3	-7.92	Ir (dπ)	49	3	28
HOMO-4	-7.94	Ir (dπ)	65	2	23
HOMO-5	-7.95	Ir (dπ)	65	2	23
HOMO-6	-7.95	Ir (dπ)	53	3	30
HOMO-7	-8.52	Ir (dσ)	95	5	0

* Note: UKS calculation provides the following compositions of the two frontier orbitals for the twisted isomer: 34% Ir, 31% C(C≡N), 29% N (αHOMO) and 85% Ir, 7% C(C≡N), 6% N (αHOMO-1).

Table S6. DFT-calculated structural parameters of the short/twisted isomer of Ir(dimen) in the electronic ground, lowest (twisted) triplet, and lowest TDDFT-calculated singlet excited states (a^1A). Atoms C1-C4 and C5-C8 refer to the two facial planes (see[1] for details). D_2 symmetry assumed for the TDDFT calculation, GS and UKS calculations without symmetry. In MeCN.

Bond (Å)	GS	UKS $^3d\sigma^*p\sigma$	TD DFT $^3d\sigma^*p\sigma$	TD DFT $^1d\sigma^*p\sigma$
Ir1-Ir2	3.251	2.861	2.845	2.883
Ir1-C1	1.959	1.963	1.963	1.965
Ir1-C2	1.959	1.964	1.962	1.966
Ir1-C3	1.959	1.963	1.963	1.965
Ir1-C4	1.959	1.964	1.962	1.966
Ir2-C5	1.959	1.964	1.963	1.966
Ir2-C6	1.959	1.963	1.962	1.965
Ir2-C7	1.959	1.964	1.963	1.966
Ir2-C8	1.959	1.963	1.962	1.965
C≡N	1.163 [a]	1.164 [a]	1.164 [a]	1.164 [a]
angle				
Ir2-Ir1-C1	92.6 [b]	93.5 [b]	93.3	93.3
Ir2-Ir1-C2	93.4 [c]	93.9 [c]	93.6	93.6
C≡N-C	168.5 [a]	166.5 [a]	167.3	168.5
C_a-Ir1-Ir2-$C_{a'}$ [c]	38.4 [d]	41.9 [d]	42.0	41.9

[a] Average of CN distances or corresponding C≡N-C angles. [b] Average of shorter Ir2-Ir1-C angles. [c] Average of larger Ir2-Ir1-C angles. [d] Average of CIr1Ir2C twist angles.

Table S7. DFT-calculated structural parameters of the long/eclipsed isomer of Ir(dimen) in the electronic ground- and lowest triplet states. Atoms C1-C4 and C5-C8 refer to the two facial planes (see[1] for details). In MeCN, no symmetry assumed.

Bond (Å)	GS	UKS a^3A
Ir1-Ir2	4.319	2.940
Ir1-C1	1.959	1.961
Ir1-C2	1.959	1.962
Ir1-C3	1.959	1.961
Ir1-C4	1.959	1.964
Ir2-C5	1.959	1.964
Ir2-C6	1.959	1.963
Ir2-C7	1.959	1.964
Ir2-C8	1.959	1.963
C≡N	1.161[a]	1.164
angle		
Ir2-Ir1-C1	90.8 [b]	95.7
Ir2-Ir1-C2	90.8	96.4
C-N-C	177.2	173.5

[a] Average of CN distances or corresponding C-N-C angles. [b] Average of shorter Ir2-Ir1-C angles.
[c] Average of larger Ir2-Ir1-C angles.

Table S8. Calculated ν(C≡N) wavenumbers (cm^{-1}) and intensities (in parenthesis, 10^3 km/mol) of the ground state (a^1A) and lowest excited singlet (b^1A) and triplet (a^3A) states of the short/twisted form of the 3:1 orientational isomer of Ir(dimen) in MeCN. Wavenumbers are scaled by 0.956.

a^1A	Exp.	b^1A[a]	Exp.	a^3A[b]	Exp.
2147 (0.0)	2128	2140(0.1)		2137(0.1)	
2147 (0.1)		2140(0.2)		2138(0.7)	
2153 (5.6)	2158	2140(0.3)		2138(0.1)	
2153 (5.7)		2143(0.1)		2141(0.7)	
2170 (0.0)		2144(5.4)		2141(5.4)	2142
2172 (0.0)		2144(6.0)	2136	2141(5.6)	
2212 (0.5)	2200	2185(0.1)		2152(2.3)	
2231 (0.0)		2220(0.0)		2222(0.1)	

[a] TDDFT calculation
[b] UKS DFT calculation

Quantum chemical calculations

Electronic structures of Ir(dimen) in ground and lowest excited states were calculated by DFT using the Gaussian 09 (G09) program package.[2] The geometry optimization of the lowest singlet and triplet excited states was performed by the time-dependent DFT (TDDFT) approach; and the lowest triplet state also was calculated by the UKS method. Geometry optimization was followed by vibrational analysis in order to characterize stationary states. Calculations performed without any symmetry constraints provided real energy minima for all investigated isomers and states. The short/twisted Ir(dimen) isomer was also optimized within the D_2 symmetry and the results were used to characterize the approximate symmetries of ν(C≡N) modes. DFT calculations employed the Perdew, Burke, Ernzerhof (PBE0) hybrid functional,[3,4] either alone or with the D3 version of Grimme's dispersion with the original D3 damping function added.[5] The MeCN solvent was described by the polarizable conductor model (PCM).[6] The following basis sets were used: double ζ 6-31g(d) basis set[7] for H; polarized triple ζ basis sets 6-311g(d)[8,9] for C, N and O atoms; and quasirelativistic effective core pseudopotentials and corresponding optimized set of basis functions for Ir.[10,11] Mayer-Mulliken bond orders were obtained by the NBO 6 program. Reported vibrational frequencies were scaled by a factor of 0.956 that provides the best match with the experimental ground-state ν(CN) bands.

DFT-calculated low-frequency vibrations

Calculations (D_2 symmetry, PCM-MeCN, harmonic approximation) on the ground-state short/twisted Ir(dimen) isomer revealed a high density of low-frequency modes, out of which those at 25, 31, and 42 cm^{-1} contain significant ν(Ir-Ir) contributions that are in all cases coupled with delocalized deformational motions of the whole molecule (including the dimen ligand backbone). There is a good match between calculated (42 cm^{-1}) and experimental[12] (48 cm^{-1}) ν(Ir-Ir) modes. Higher ν(Ir-Ir) wavenumbers were calculated (TDDFT) in the $^1d\sigma^*p\sigma$ and $^3d\sigma^*p\sigma$ excited states: 77, 96, and 120 cm^{-1} and 78, 98, and 128 cm^{-1}, respectively.

Orientational isomerism

Besides deformational isomerism, where the two forms differ in the Ir-Ir distance and the twist angle, Ir(dimen) also can exist in several "orientational isomers" that differ in the "head-to-tail" relative orientations of the dimen ligands: 4:0 (all aligned), 3:1, *cis*-2:2, and *trans*-2:2. The respective DFT-calculated free energies of Ir(dimen) orientational isomers (relative to the most stable isomer, MeCN, 293 K) are 0.077, 0.011, 0.003, and 0.0 eV for the long/eclipsed deformational isomer and 0.005, 0.0, 0.049, and 0.032 eV for the short/twisted isomer.[1] The actual solution composition is not known and may vary with synthetic conditions. Crystal structures[13] show disordered dimen orientations, which correspond to mixtures of orientational isomers. In this work, we present computational results for the *trans*-2:2 isomer. For comparison, we have performed calculations also on the 3:1 isomer. The calculated ground- and excited-state structures of the $Ir_2(C{\equiv}N{-})_8$ part of the molecule, as well as molecular orbitals and IR spectra are nearly identical with those obtained for the *trans*-2:2 case. Calculated ground- and excited-state $\nu(C{\equiv}N)$ wavenumbers of the 3:1 isomer are listed in Table S8.

References

1. Záliš, S.; Hunter, B. M.; Gray, H. B.; Vlček, A., Electronic Structures of Reduced and Superreduced Ir_2(1,8-diisocyanomenthane)$_4^{n+}$ Complexes. *Inorg. Chem.* **2017,** *56*, 2874−2883.

2. Frisch, M. J.; Trucks, G. W.; Schlegel, H. B.; Scuseria, G. E.; Robb, M. A.; Cheeseman, J. R.; Scalmani, G.; Barone, V.; Mennucci, B.; Petersson, G. A.; Nakatsuji, H.; Caricato, M.; Li, X.; Hratchian, H. P.; Izmaylov, A. F.; Bloino, J.; Zheng, G.; Sonnenberg, J. L.; Hada, M.; Ehara, M.; Toyota, K.; Fukuda, R.; Hasegawa, J.; Ishida, M.; Nakajima, T.; Honda, Y.; Kitao, O.; Nakai, H.; Vreven, T.; Montgomery, J. A., Jr.; Peralta, J. E.; Ogliaro, F.; Bearpark, M.; Heyd, J. J.; Brothers, E.; Kudin, K. N.; Staroverov, V. N.; Kobayashi, R.; Normand, J.; Raghavachari, K.; Rendell, A.; Burant, J. C.; Iyengar, S. S.; Tomasi, J.; Cossi, M.; Rega, N.; Millam, J. M.; Klene, M.; Knox, J. E.; Cross, J. B.; Bakken, V.; Adamo, C.; Jaramillo, J.; Gomperts, R.; Stratmann, R. E.; Yazyev, O.; Austin, A. J.; Cammi, R.; Pomelli, C.; Ochterski, J. W.; Martin, R. L.; Morokuma, K.; Zakrzewski, V. G.; Voth, G. A.; Salvador, P.; Dannenberg, J. J.; Dapprich, S.; Daniels, A. D.; Farkas, O.; Foresman, J. B.; Ortiz, J. V.; Cioslowski, J.; Fox, D. J. *Gaussian 09, Revision D.01*, Gaussian 09, Revision C.01, Gaussian, Inc.: Wallingford CT, 2009.

3. Perdew, J. P.; Burke, K.; Ernzerhof, M., Generalized Gradient Approximation Made Simple. *Phys. Rev. Lett.* **1996,** *77*, 3865-3868.

4. Adamo, C.; Barone, V., Toward reliable density functional methods without adjustable parameters: The PBE0 model. *J. Chem. Phys.* **1999,** *110*, 6158-6170.

5. Grimme, S.; Antony, J.; Ehrlich, S.; Krieg, H., A consistent and accurate ab initio parameterization of density functional dispersion correction (DFT-D) for the 94 elements H-Pu. *J. Chem. Phys.* **2010,** *132*, 154104.

6. Tomasi, J.; Mennucci, B.; Cammi, R., Quantum Mechanical Continuum Solvation Models. *Chem. Rev.* **2005,** *105*, 2999-3093.
7. Ditchfield, R.; Hehre, W. J.; Pople, J. A., Self-Consistent Molecular Orbital Methods. 9. Extended Gaussian-type basis for molecular-orbital studies of organic molecules. *J. Chem. Phys.* **1971,** *54*, 724-728.
8. Raghavachari, K.; Binkley, J. S.; Seeger, R.; Pople, J. A., Self-consistent molecular orbital methods. XX. A basis set for correlated wave functions *J. Chem. Phys.* **1980,** *72*, 650-654.
9. McLean, A. D.; Chandler, G. S., Contracted Gaussian-basis sets for molecular calculations. 1. 2nd row atoms, Z=11-18. *J. Chem. Phys.* **1980,** *72*, 5639-5648.
10. Andrae, D.; Häussermann, U.; Dolg, M.; Stoll, H.; Preuss, H., Energy-adjusted ab initio pseudopotentials for the second and third row transition elements. *Theor. Chim. Acta* **1990,** *77*, 123-141.
11. Martin, J. M. L.; Sundermann, A., Correlation consistent valence basis sets for use with the Stuttgart–Dresden–Bonn relativistic effective core potentials: The atoms Ga–Kr and In–Xe. *J. Chem. Phys.* **2001,** *114*, 3408-3420.
12. Hartsock, R. W.; Zhang, W.; Hill, M. G.; Sabat, B.; Gaffney, K. J., Characterizing the Deformational Isomers of Bimetallic $Ir_2(dimen)_4^{2+}$ (dimen = 1,8-diisocyano-p-menthane) with Vibrational Wavepacket Dynamics. *J. Phys. Chem. A* **2011,** *115*, 2920–2926.
13. Exstrom, C. L.; Britton, D.; Mann, K. R.; Hill, M. G.; Miskowski, V. M.; Schaefer, W. P.; Gray, H. B.; Lamanna, W. M., Structures of $[M_2(dimen)_4](Y)_2$ (M = Rh, Ir; dimen = 1,8-Diisocyanomenthane; Y = PF_6, Tetrakis[3,5-bis(trifluoromethyl)phenyl]borate, $B(C_6H_5)_4$) Crystals Featuring an Exceptionally Wide Range of Metal-Metal Distances and Dihedral Twist Angles. *Inorg. Chem.* **1996,** *35*, 549-550.